Carbohydrate Polymers 97 (2013) 243–251

Contents lists available at SciVerse ScienceDirect

Carbohydrate Polymers

journal homepage: www.elsevier.com/locate/carbpol

Cellulose nanofibers/reduced graphene oxide flexible transparent conductive paper

Kezheng Gao, Ziqiang Shao*, Xue Wu, Xi Wang, Jia Li, Yunhua Zhang, Wenjun Wang, Feijun Wang

School of Materials Science & Engineering, Beijing Institute of Technology, Beijing 100081, PR China

ARTICLE INFO

Article history:
Received 18 September 2012
Received in revised form 27 February 2013
Accepted 24 March 2013
Available online 29 March 2013

Keywords:
Flexible transparent conductive paper
Cellulose nanofiber
Reduced graphene oxide
Layer-by-layer assembly

ABSTRACT

The cellulose nanofibers (CNFs) paper exhibit high visible light transmittance, high mechanical strength, and excellent flexibility. Therefore, CNFs paper may be an excellent substrate material for flexible transparent electronic devices. In this paper, we endeavor to prepare CNFs-based flexible transparent conductive paper by layer-by-layer (LbL) assembly using divalent copper ions (Cu^{2+}) as the crosslinking agent. The thickness of the reduced graphene oxide (RGO) active layer in the CNFs paper can be controlled by the cycle times of the LbL assembly. CNFs/$[RGO]_{20}$ paper has the sheet resistances of ~2.5 kΩ/□, and the transmittance of about 76% at a wavelength of 550 nm. Furthermore, CNFs/$[RGO]_{20}$ paper inherits the excellent mechanical properties of CNFs paper, and the ultimate strength is about 136 MPa. CNFs-based flexible transparent conductive paper also exhibits excellent electrical stability and flexibility.

1. Introduction

Flexible transparent conductive films will be widely applied in the flexible consumer electronics, smart clothing, energy harvesting, and sensors in the future. Next-generation flexible transparent conductive films not only must retain their high-performance (transmittance, conductivity, flexibility), but also needs have light weight, low cost, and capability for large-scale manufacturing. Most importantly, these materials should have environmentally friendly features. However, traditional transparent conductive films (such as ITO) cannot fulfill the requirements of the next-generation flexible electronic device because they are rigid and fragile (Kumar & Zhou, 2010). In recent years, flexible transparent conductive films have been successfully prepared, such as some conductive active materials including metal oxides semiconductors (Nomura et al., 2004), conducting polymers (Kao et al., 2009), carbon nanotubes (Kaempgen, Duesberg, & Roth, 2005), graphene (Chang et al., 2010), metallic nanowires (Rathmell & Wiley, 2011; Yu et al., 2011). They are deposited on a flexible plastic substrate (such as PET) by spin-coating, filtration, Langmuir–Blodgett assembly, dip-coating, etc. However, many plastic materials used as substrate for the flexible transparent conductive film have the very important shortcoming of large coefficients of thermal expansion (CTE, more than 1.3×10^{-5}/K) (MacDonald, 2004), which is incompatible with the conductive active materials. So, the conductive materials on the plastic substrate will be damaged by temperature changes during the preparation of the flexible transparent conductive film (Nogi, Iwamoto, Nakagaito, & Yano, 2009). Furthermore, plastics may be limited as the substrate of the flexible transparent conductive film in the future because these plastics are generally considered environmentally unfriendly. At present, it is still a great challenge to find an environmentally friendly material with superior performance to the flexible transparent conductive substrate.

Cellulose nanofiber is a kind of ordered aggregation of cellulose macromolecules (Holt, Stoyanov, Pelan, & Paunov, 2010). They have some excellent properties such as high aspect ratio (Saito, Kimura, Nishiyama, & Isogai, 2007), high crystallinity (Eichhorn, 2011), low coefficient of thermal expansion (Nishino, Matsuda, & Hirao, 2004), low density, and high elastic modulus (Iwamoto, Kai, Isogai, & Iwata, 2009). Therefore, the preparation of cellulose nanofibers has aroused worldwide interest. Many groups attempt to obtain the uniform cellulose nanofibers by acid hydrolysis (Dong, Revol, & Gray, 1998), enzymatic hydrolysis (Paakko et al., 2008), and mechanical shear method (Chen, Yu, Li, Liu, & Li, 2011). However, complete individualization of wood cellulose to 3–4 nm wide nanofibers without damages has not yet been achieved. Furthermore, the methods mentioned above also have some problems such as low recovery ratios, high energy consumption, and so on. In recent years, the cellulose nanofibers (at least a few microns long and 3–4 nm wide) have been successfully prepared by TEMPO-mediated oxidation of never-dried softwood cellulose successive gentle mechanical disintegration (Saito et al., 2009). This kind cellulose nanofiber can easily suspend in the water because of the

* Corresponding author. Tel.: +86 010 68941797x609; fax: +86 010 68941797x601.
E-mail addresses: gaokezheng@126.com (K. Gao), shaoziqiang@263.net (Z. Shao).

0144-8617/$ – see front matter © 2013 Published by Elsevier Ltd.
http://dx.doi.org/10.1016/j.carbpol.2013.03.067

electrostatic repulsion between the abundant ionized carboxyl groups at C6 on the surface of the cellulose nanofibers in neutral aqueous solution. The suspension of cellulose nanofibers has good film forming properties (Saito, Uematsu, Kimura, Enomae, & Isogai, 2011). The CNFs paper has excellent transmittance (about 90%, at 550 nm), low thermal expansion (2.7×10^{-6}/K) (Fukuzumi, Saito, Wata, Kumamoto, & Isogai, 2009), which is as low as glass, high mechanical strength, high oxygen-barrier property, outstanding flexibility and the refractive index is 1.545 ± 0.002 at room temperature (Isogai, Saito, & Fukuzumi, 2011). Therefore, in our opinion, CNFs paper will perhaps become an extremely important base material in the next-generation flexible electronic devices.

Layer-by-layer assembly is one of a few techniques, which can control over the materials' structure on a nano-scale, using of non-covalent interactions, such as hydrogen bonds, π–π stacking interactions, and electrostatic forces, by the substrate's alternate exposure into the different dilute solution (Shim et al., 2009). Recently, the LbL assembly technique has been used for the preparation of transparent conductive films (Zhu, Shim, Di Prima, & Kotov, 2011), because the thickness of the conductive active layer can be effectively and easily controlled. However, owing to the many hydrophilic oxygenated functionalized groups (carboxyl, hydroxyl, and epoxy group) in the GO nanosheets, the strong electrostatic repulsion between the GO nanosheets prevent the spontaneous formation of the interconnected GO nanosheets film (Cote, Kim, & Huang, 2009). This seems to imply that the LbL assembly technique is not suitable for preparing the graphene-based flexible transparent conductive film without the assistance of other substances. In recent years, transparent conductive films have been prepared by spin-coating the complex between oxidized CNTs and GO using divalent metal ions. The CNTs/RGO hybrid film has superior photoelectric performance (Liu, Feng, Xie, & Ye, 2011). This indicates that GO nanosheets can be strongly interconnected with each other by divalent metal ion's coordination. Furthermore, the high-quality interface will be formed between the CNFs and GO active layer by the divalent metal ion's coordination because the large number of ionized carboxyl groups in the CNFs paper surface (Okita, Saito, & Isogai, 2010). This high-quality interface may be maintained after reduction. This is beneficial to the stability of the CNFs-based transparent conductive paper. Therefore, the CNFs/$[RGO]_n$ transparent conductive paper prepared by LbL assembly will show the excellent photoelectric performance.

Therefore, we have endeavored to prepare CNFs-based flexible transparent conductive paper by LbL assembly technique using divalent copper ions as crosslinking agent. The thickness of RGO active layer in the CNFs paper can be effectively controlled by the cycle times of the LbL assembly. HI acid is selected as the chemical reducing agent in our case (Pei, Zhao, Du, Ren, & Cheng, 2010).

2. Experimental

2.1. Materials

Graphite flake (<300 mesh), sulfuric acid (98%), chlorhydric acid (36 wt%), hydrogen peroxide (36 wt%), hardwood bleached kraft pulps in the never-dried wet state with 78% water content, TEMPO (2,2,6,6-tetramethylpiperidine-1-oxyl radical), sodium bromide, sodium hypochlorite solution. All the chemicals are used without further purification.

2.2. Preparation of cellulose nanofibers dispersion

CNFs were prepared according to the literature methodology reported by Isogai (Saito, Nishiyama, Putaux, Vignon, & Isogai, 2006), and described in brief as follows: cellulose fibers (2 g) were suspended in water (400 mL) containing TEMPO (0.033 g) and sodium bromide (0.33 g). The oxidation reaction was started by adding the desired amount of the NaClO solution (15 mmol/g cellulose). The pH of the reaction solution was maintained to be 10.00 at 10 °C by adding 0.5 M NaOH for 6 h. The oxidized cellulose was thoroughly washed with water by filtration. 2 mg/mL oxidized cellulose/water slurries were sonicated for 15 min using an ultrasonic generator (SCIENTZ-II D, Ningbo Scientz Biotechnology Co., Ltd., China) with a probe tip15 cm in diameter at an output power of 300 W in an ice bath. Cellulose nanofibers dispersions were centrifuged at 10,000 rpm for 10 min to remove the unfibrilated cellulose. The transparent cellulose nanofibers dispersion was stored at 4 °C before used.

2.3. Preparation of graphene oxide dispersion

GO nanosheets were prepared by the modified Hummers and Tung's method reported elsewhere (Hummers & Offeman, 1958; Tung, Allen, Yang, & Kaner, 2009). Briefly, graphite powder (6 g) was added into 100 mL beaker containing concentrated H_2SO_4 (25 mL), $K_2S_2O_8$ (5 g), P_2O_5 (5 g) with continuous stirring at 80 °C. The resulting mixture was kept at 80 °C for 4.5 h in oil bath, then DI water (about 1 L) was added to the resulting mixture and left overnight. Pretreated graphite was thoroughly washed with water by filtration to remove all soluble substances and then dried in the oven at 60 °C. Pretreated graphite was added into 1000 mL beaker containing concentrated H_2SO_4 (230 mL) in ice bath. $KMnO_4$ (30 g) was added slowly to dissolve completely. The resulting mixture was allowed to react at 35 °C for about 2 h, and then 460 mL DI water was slowly added. In the process of adding water, the temperature of the mixture was remained constant. Another 1.4 L DI water was added to the mixed solution with continuous stirring at room temperature for 2 h afterward, 25 mL of 30% H_2O_2 was added to the mixture with continuous stirring at room temperature. The color of the mixed solution becomes golden yellow. The resulting mixture was stood for about 12 h and then the supernatant was decanted. The graphite oxide was thoroughly washed with 5% HCl solution and then DI water to remove all soluble substances. 8 mg/mL graphite oxide was sonicated for 30 min using an ultrasonic generator at an output power of 600 W. The graphene oxide solution was centrifuged at 10,000 rpm for 5 min to remove the unexfoliated graphite oxide. The inorganic ions in the graphene oxide suspension were removed by dialysis.

2.4. Preparation of CNFs/$[RGO]_n$ flexible transparent conductive paper by layer-by-layer assembly

The CNFs paper can be prepared by the static evaporation of the water in the polytetrafluoroethylene (PTFE) petri dishes at 60 °C for 4 h and then at room temperature for desired time. The CNFs paper was first dipped into the Cu^{2+} solution (1 mg/mL, pH 4.5) for 1 min, rinsed by the DI water, and then dried with hot air (about 65 °C). Subsequently, the paper was dipped into the GO suspension (1 mg/mL, pH 4.5) for 1 min, followed by similar rinsing and drying. The above cycle can be repeated until obtain desired number of cycles. The paper will be called CNFs/$[Cu^{2+}/GO]_n$. CNFs/$[Cu^{2+}/GO]_n$ paper was reduced by HI acid at 80 °C for 10 s and called CNFs/$[RGO]_n$ paper where n is the number of cycles.

2.5. Characterization

The chemical characterizations of the samples were examined by Fourier transform infrared spectrometry (Nicolet 6700 infrared spectrometer, USA). Morphology of the cellulose nanofibers and GO nanosheets were characterized by transmission electron microscope (JEM-200CX, Japan) at an acceleration voltage of

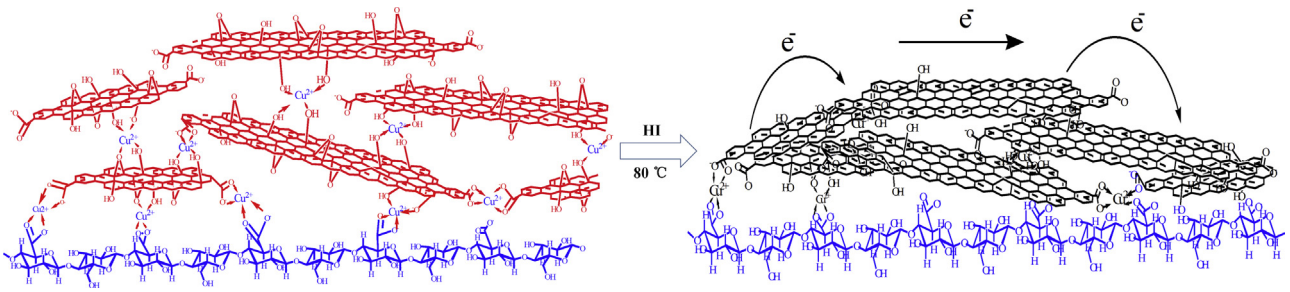

Fig. 1. Schematic diagram of CNFs/$[Cu^{2+}/GO]_n$ and CNFs/$[RGO]_n$ paper with Cu^{2+} as crosslinking agent.

120 kV. XRD measurements of the Hardwood pulps, CNFs paper, CNFs/$[Cu^{2+}/GO]_{20}$ paper, and CNFs/$[RGO]_{20}$ paper were performed on a D8 Advance (Bruker Co., Germany) X-ray diffractometer (40 kV, 40 mA) with Cu Ka radiation ($\lambda = 0.154$ nm) in the 2θ range of 10–60° with a step interval of 0.02°. The absorbance and transparency of the CNFs paper, CNFs/$[Cu^{2+}/GO]_n$ paper, and CNFs/$[RGO]_n$ paper were measurement by Hitachi U-1500 UV spectrometer. Surface morphology of the CNFs paper, CNFs/$[RGO]_{20}$ paper was acquired by a tapping mode AFM (SPM-9600, Shimadzu). Raman spectra was collected from 100 to 4000 cm^{-1} using an NRS 300 laser Raman spectrometer (Jobin Yvon LabRam 300) with an excitation wavelength of 633 nm at room temperature. The electrical conductivities of all the CNFs/$[RGO]_n$ paper were assessed by the Keithley 4200 semiconductor characterization system. Energy dispersive spectrometer (EDS) measurements were carried out on the FESEM. Mechanical properties of transparent conductive films were assessed by INSTRON 1185 universal testing machine (USA). X-ray photoelectron spectroscopy (XPS) was conducted on a PHI Quantera II instrument with Al Ka as the X-ray source set at 24.8 W. Low-resolution spectra were recorded using 280 eV analyzer pass energy and high-resolution regional spectra were obtained using 26 eV analyzer pass energy. The depth profile of sample was obtained using 2 kV argon ion sputter gun. All binding energies were referenced to the C1s neutral carbon peak at 284.8 eV.

3. Results and discussion

The detailed characterization of the GO nanosheets and the CNFs are provided in supplementary material. Owning to the strong electrostatic repulsion between the GO nanosheets (Bai, Li, Wang, & Shi, 2011), it is almost impossible for GO nanosheets to spontaneously assemble into a precise hierarchy in the CNFs paper by the LbL assembly under unconstrained conditions. Recent study shows that divalent metal ion's (such as divalent Cu^{2+} ions) coordination is one of the most effective ways of interconnecting GO nanosheets with CNFs (or GO nanosheets) by the oxygen-containing functional groups (mainly carboxylate groups on the surface of CNFs) (Park et al., 2008). GO nanosheets containing different or the same layers may be closely locked each other by the divalent Cu^{2+} ions crosslinking agent during LbL assembly process. Therefore, The flexible transparent conductive CNFs/$[RGO]_n$ paper are prepared by LbL assembly using divalent metal ions (Cu^{2+}) as crosslinking agent, and the mechanism model as shown in Fig. 1. The most important influencing factors of LbL assembly are the pH value and the Cu^{2+} concentration. The optimum of the pH value and the Cu^{2+} concentration are 4.5 and 1 mg/mL respectively (Fig. S7). Fig. 2 shows the digital pictures of CNFs, CNFs/$[Cu^{2+}/GO]_{20}$, CNFs/$[RGO]_{20}$ paper. All the papers show excellent flexibility and little color changes.

Fig. 3a presents FT-IR spectra of the CNFs, CNFs/$[Cu^{2+}/GO]_{20}$, and CNFs/$[RGO]_{20}$ paper. The characteristic C=O stretching peak of sodium carboxyl groups for the CNFs, CNFs/$[Cu^{2+}/GO]_{20}$, CNFs/$[RGO]_{20}$ paper appears at 1608 cm^{-1}. However, the C=O stretching (carboxyl/carbonyl) peak of the CNFs/$[Cu^{2+}/GO]_{20}$ paper also appears at 1720 cm^{-1} may be because carboxylic acid coordinates between carboxylic acid and Cu^{2+} (Creager & Steiger, 1995), which indicate that the divalent Cu^{2+} ion is an effective binder between GO nanosheets and CNFs (or GO nanosheets). The CNFs/$[RGO]_{20}$ paper exhibit increase in C=O stretch intensity (1720 cm^{-1}) as well as decreases C=O stretch intensity (1608 cm^{-1}) maybe because the divalent metal ions are unmasked and the sodium carboxyl groups of CNFs/$[RGO]_{20}$ paper may be converted to free carboxyl groups by HI acid after reduction. The C=O stretching peak at 1720 cm^{-1} indicates that majority of carboxyl groups (including residual carboxyl of RGO nanosheets) in the CNFs/$[RGO]_{20}$ paper form hydrogen bonds. Therefore, the high-quality interface between the CNFs and RGO active layer may be formed by hydrogen bonds. The metal ions can lead to ring-opening of the epoxide. Therefore, the relative intensity of the hydroxyl and alkoxide C—O stretches of CNFs/$[Cu^{2+}/GO]_{20}$ paper at 1161 cm^{-1} slight increase.

The UV–vis absorbance spectra of GO and RGO exhibit the characteristic absorption peak at 230 nm and 266 nm respectively, which are attributable to $\pi \rightarrow \pi^*$ transitions of aromatic C—C bonds (Marcano et al., 2010). However, CNFs paper does not show any characteristic absorption peaks between 200 nm and 800 nm. So,

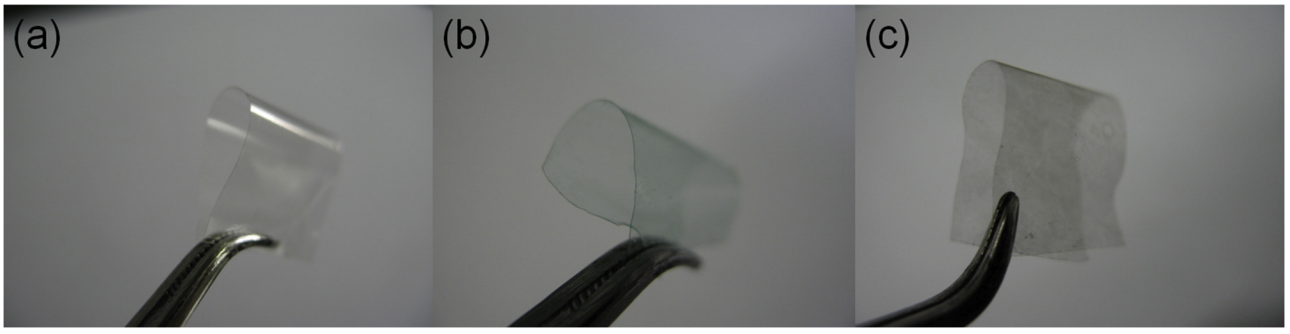

Fig. 2. Digital pictures of CNFs (a), CNFs/$[Cu^{2+}/GO]_{20}$ (b), CNFs/$[RGO]_{20}$ (c) paper using canon camera under ambient conditions.

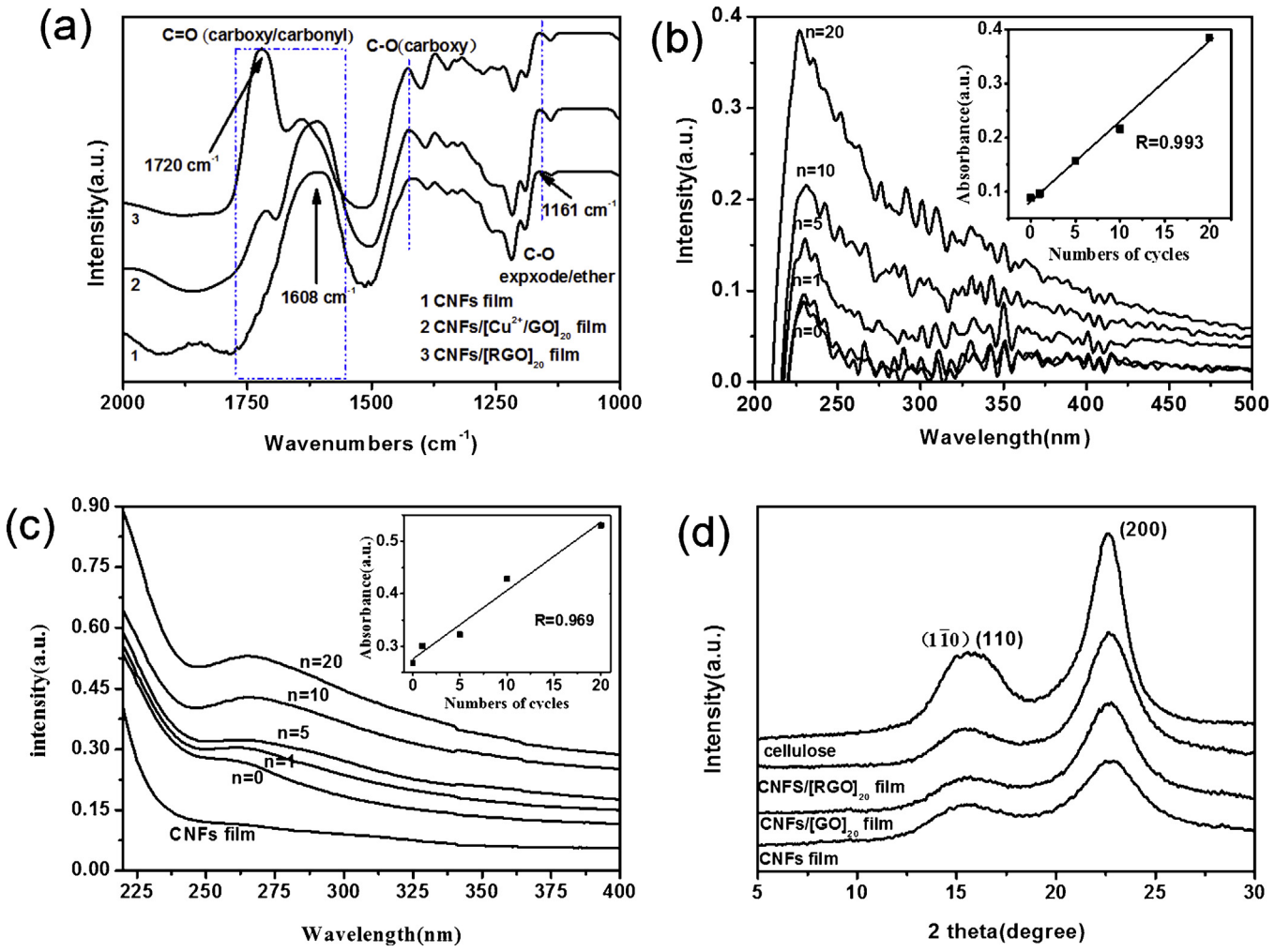

Fig. 3. FT-IR spectra of CNFs, CNFs/$[Cu^{2+}/GO]_{20}$ and CNFs/$[GO]_{20}$ paper (a) directly test the dried samples, UV/vis absorbance spectra of (b) CNFs/$[GO]_n$ paper and (c) CNFs/$[RGO]_n$ paper with different numbers of graphene bilayers, Insets show the linear relation between the absorbance at the characteristic peak (230, 260 nm for CNFs/$[GO]_n$ paper, and CNFs/$[RGO]_n$ paper respectively) and the number of bilayers. (d) XRD spectra of cellulose, CNFs paper, CNFs/$[GO]_{20}$ paper and CNFs/$[RGO]_{20}$ paper with Cu Ka radiation ($\lambda = 0.154$ nm) and a step interval of 0.02°.

gradual growth process of GO or RGO active layer in the CNFs paper can be monitored by UV–vis spectroscopy. Fig. 3b shows the UV–vis absorbance spectra of CNFs/$[Cu^{2+}/GO]_n$ paper. The absorption intensity of CNFs/$[Cu^{2+}/GO]_n$ paper at 230 nm is linearly proportional to the cycle times (Fig. 3b inset). This indicates that LbL assembly can accurately control the growth process of the active layer, and the Cu^{2+} is an effective crosslinking agent for GO nanosheets. CNFs/$[RGO]_n$ papers are prepared by reducing of CNFs/$[Cu^{2+}/GO]_n$ paper with 55% hydroiodic (HI) acid for 10 s at 80 °C (HI acid is a highly efficient reducing agent of GO nanosheets. More importantly, it also can maintain good integrity and flexibility of the RGO film during the reducing process (Zhao, Pei, Ren, Gao, & Cheng, 2010)). After chemical reduction, the characteristic absorption peak of GO nanosheets red shifts to 266 nm (Fig. 3c), which indicates the successful restoration of conjugated C=C bonds of graphene. The characteristic absorption peak intensity of RGO increase linearly with the number of cycles (inset of Fig. 3c). The linear relationship between absorbance and number of cycles indicates that the integrity of RGO active layer in the CNFs/$[RGO]_n$ paper can be effectively maintained after reduction.

Owing to the retention of the original cellulose I crystalline structure is retained; the CNFs paper has high mechanical strength, low thermal expansion, excellent flexibility, and good heat-transfer properties. However, during the reducing process, HI acid is used as the reducing agent. Cellulose I allomorph may be destroyed by HI acid at 80 °C. In order to maintain the excellent mechanical properties of CNFs paper, the reducing time should be controlled within 10 s. Fig. 3d shows X-ray diffraction patterns of the original untreated cellulose fibers, CNFs, CNFs/$[GO]_{20}$, and CNFs/$[RGO]_{20}$ paper. All the diffractograms show two peaks around $2\theta = 15.6°$ and 22.5°, which are believed to represent the typical cellulose I crystalline structure (Saito & Isogai, 2004). However, the intensity of diffraction peak changed may be because of the interaction between CNFs and GO (or RGO) using Cu^{2+} ion's coordination by the carboxylate groups on the surfaces of CNFs. This indicates that the crystal integrity has been maintained after reduce by HI acid within 10 s. Therefore, the CNFs/$[RGO]_{20}$ flexible transparent conductive paper will inherit many of the excellent performances of CNFs paper such as high mechanical strength as well as excellent flexibility.

The prerequisite of RGO-based transparent conductive films is that the GO nanosheets should be highly effective and sufficiently reduced. Although, HI acid is a fast, effective reducing agent of GO nanosheets, the reducing process is a gradual outer-to-inner diffusion process for HI acid. Therefore, the reduction time should be controlled strictly in order to get the high-performance CNFs/$[RGO]_n$ transparent conductive paper. However, CNFs/$[Cu^{2+}/GO]_{20}$ paper is reduced in only 10 s in our case. Can

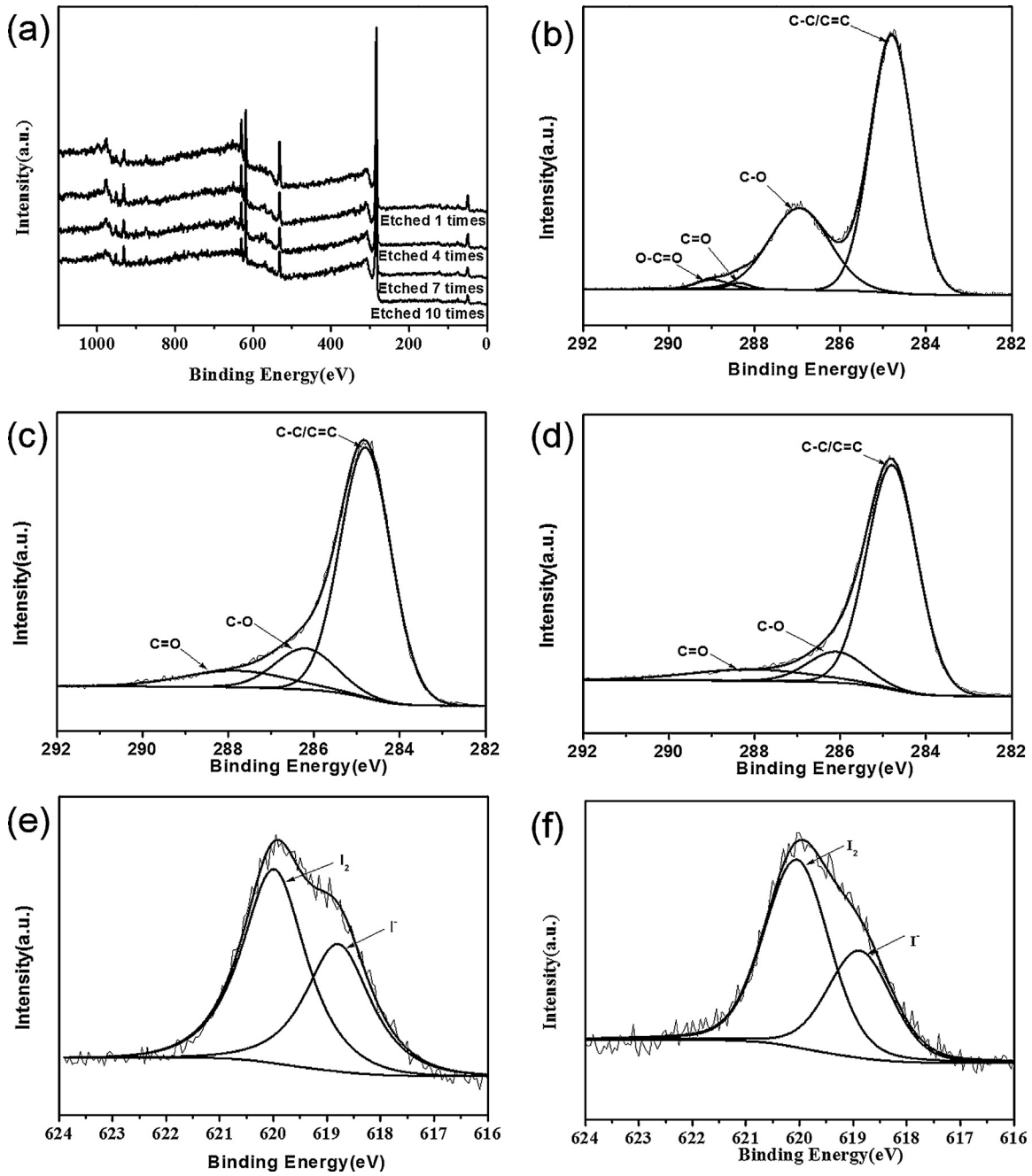

Fig. 4. (a) XPS wide region scan survey spectrum of CNFs/$[RGO]_{20}$ paper with etched 1, 4, 7, and 10 times. High-resolution XPS C1 spectra of CNFs/$[GO]_{20}$ paper (b), etched 1 times (c), etched 10 times (d). High-resolution XPS I 3d5/2 spectra of etched 1 times (e) and etched 10 times (f), Al Ka as the X-ray source set at 24.8 W and the depth profile of sample was obtained using 2 kV argon ion sputter gun.

the GO nanosheets in the CNFs/$[Cu^{2+}/GO]_{20}$ paper be reduced sufficiently? X-ray photoelectron spectroscopy (XPS) etching technique can be used to study the elements' depth profile of the CNFs/$[RGO]_{20}$ paper. In order to investigate the reduction degree of GO at different depths of the CNFs/$[RGO]_{20}$ paper, XPS etching technique is employed. Fig. 4a provides the spectra of the CNFs/$[RGO]_{20}$ paper with etched 1, 4, 7, and 10 times from 0 to 1100 eV. Notable peaks are observed at binding energy of 49, 284, 532, 619, 630, and 932 eV, corresponding to I $4d_{5/2}$, C 1s, O 1s, I $3d_{5/2}$, I $3d_{3/2}$, Cu $2p_{3/2}$, respectively. The full-scan spectra of the CNFs/$[RGO]_{20}$ paper is virtually unchanged with the increase of etching times. In order to research detailed reduction degree of GO at different depths, the high-resolution XPS C 1s and I $3d_{5/2}$ spectra of the CNFs/$[RGO]_{20}$ paper are performed after each etched. Fig. 4b–d shows the high-resolution XPS C 1s spectra of CNFs/$[GO]_{20}$ paper and CNFs/$[RGO]_{20}$ paper etched 1, 10 times. The curves are fitted considering the following contributions: C=C/C—C (284.7 eV), C—O (286.9 eV), C=O (288.3 eV), O—C=O (288.9 eV) for CNFs/$[GO]_{20}$ paper. While, for CNFs/$[RGO]_{20}$ paper, The curves are fitted considering the following contributions: C=C/C—C (284.8 eV), C—O (286.2 eV), C=O (287.9 eV). The high-resolution XPS C 1s spectra changes distinctly after reduction, as shown by a single peak. The C/O atomic ratio of CNFs/$[GO]_{20}$ paper increases from about 3.8 to about 12 after reduction. The C/O atomic ratio of the CNFs/$[RGO]_{20}$ paper etched 10 times is still as high as about 12. These results clearly indicate that almost all oxygen-containing groups of CNFs/$[RGO]_{20}$ paper have been removed and the conjugated C=C bonds become dominant. The iodine anions are the main

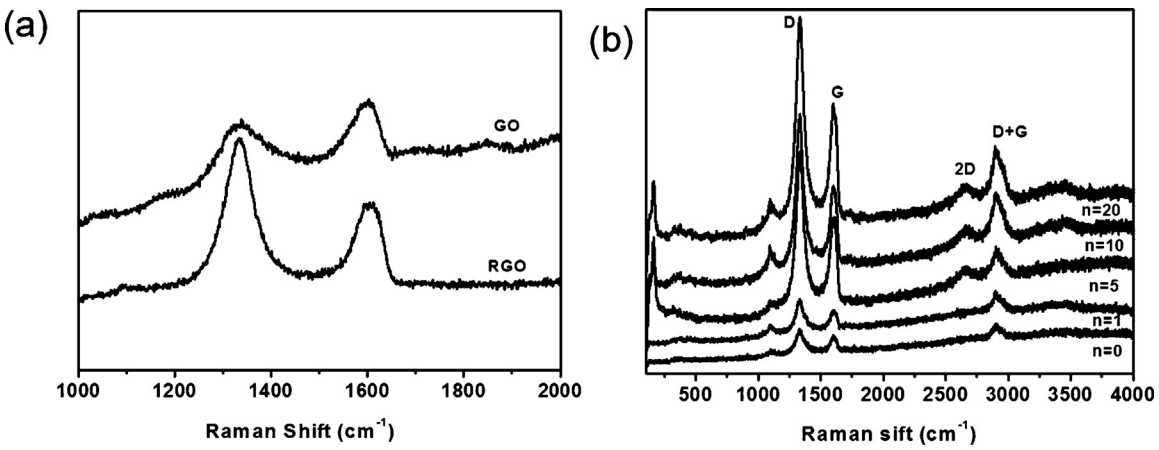

Fig. 5. (a) Raman spectra of GO, CNFs/$[RGO]_{20}$. Raman spectra of CNFs/$[RGO]_n$ with different numbers of graphene bilayers (b) with an excitation wavelength of 633 nm at room temperature.

reducing agent, which donate electrons to achieve the restoration of the conjugated structure of graphene. So, the distribution profile of iodine at different depths can also be used to characterize the reduction degree of GO nanosheets. The I $3d_{5/2}$ (centered at 619 eV) peaks of CNFs/$[RGO]_{20}$ paper etched 1 and 10 times are shown in Fig. 4e and f. Residual iodine is mainly present in two states: I_2 and I^-. The ratio of peak from I^- to peak from I_2 decreases from about 0.67(etched 1 times) to about 0.56 (etched 10 times). This indicates that there are still large amounts of iodine anion in the interior of the RGO conductive active layer. The oxygen-containing groups of the CNFs/$[RGO]_{20}$ paper can be further reduced by those excess iodide ions. Therefore, GO nanosheets at different depths of the CNFs/$[RGO]_{20}$ paper can be effectively and entirely reduced by HI within 10 s.

Raman spectroscopy is an effective structural testing technique of carbon-based materials. The reduction degree of GO, quality and number of RGO layers can be assessed by Raman spectroscopy (Graf et al., 2007). G and D peaks are both excitated by vibration of sp^2 carbon. Raman spectroscopy of the GO and RGO nanosheets are shown in Fig. 5a. G peak of the GO nanosheets red shifts from 1596 to 1605 after chemical reduction because the decrease of the content of sp^2 carbon and restore the conjugated structure of graphene. The ratio (I_D/I_G), which always used to assess the degree of disorder, increased from ~0.9 to ~1.3 after GO nanosheets is reduced.

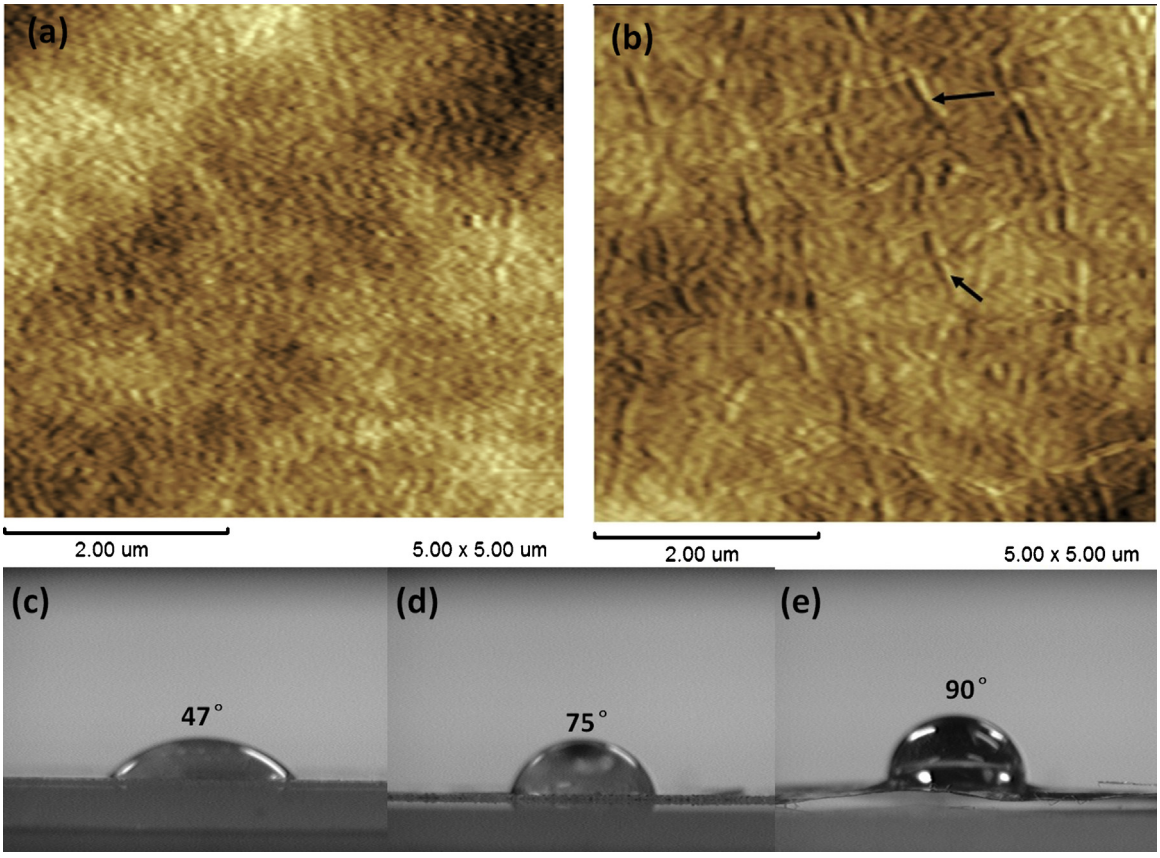

Fig. 6. AFM images of CNFs film (a) and CNFs/$[RGO]_{20}$ film (b) with the tapping mode, the contact angle of CNFs (c), CNFs/$[GO]_{20}$(d), CNFs/$[RGO]_{20}$(e) at ambient conditions.

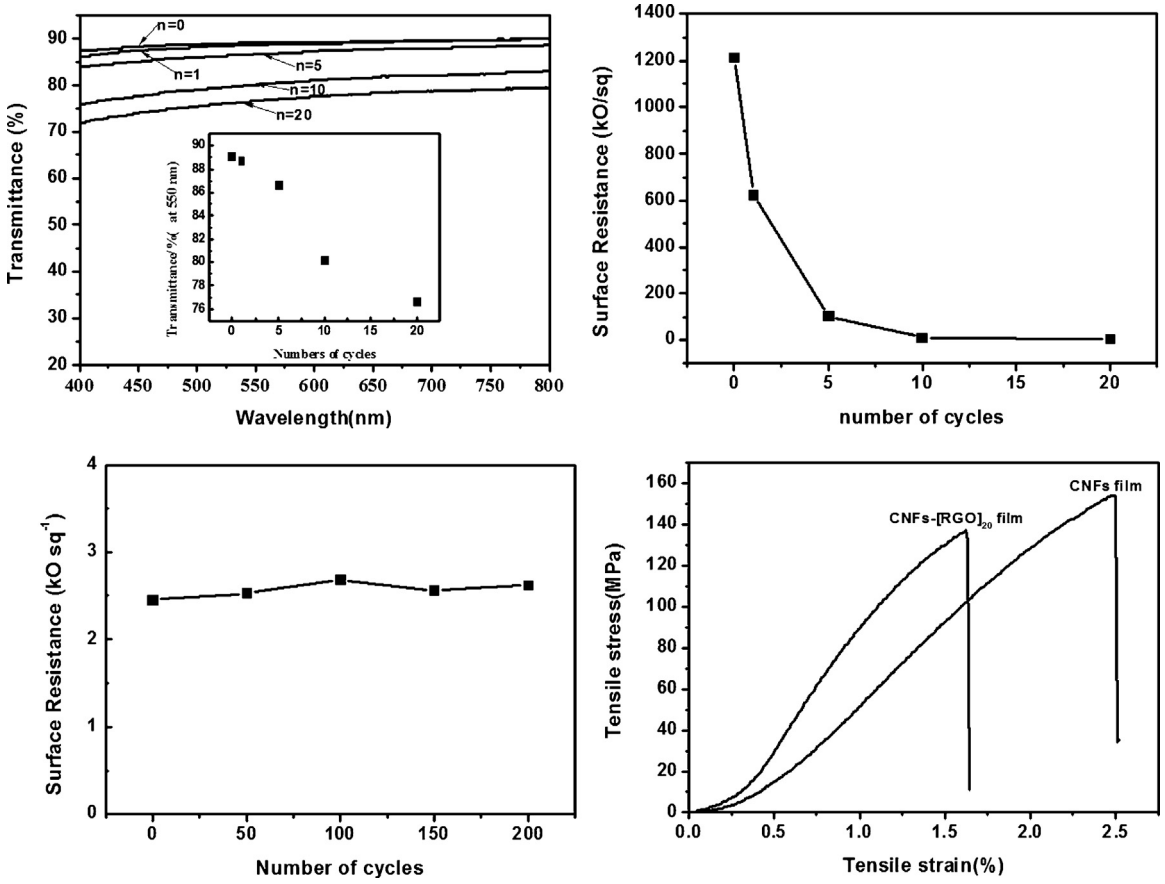

Fig. 7. Transmission of CNFs/$[RGO]_n$ paper with different numbers of graphene bilayers, insets show the linear relation between the transmission at 550 nm and the number of bilayers, the transmittance values of only one sided paper (a). Sheet resistance of CNFs/$[RGO]_n$ paper with different number of cycles (b) and number of bends (c) at ambient conditions. (d) Stress–strain curves of the CNFs paper and the CNFs/$[RGO]_{20}$ paper with a tensile rate of 1 mm/min.

This result indicates that RGO compared with GO becomes more disordered. Fig. 5b shows the evolution of Raman spectroscopy of CNFs/$[RGO]_n$ paper with the increase number of cycles. The characteristic G and D peak of CNFs/$[RGO]_n$ paper appears centered at 1605 and 1333 cm^{-1} respectively, and the intensity of G and D peak increases significantly with the increase number of cycles. However, the ratio (I_D/I_G) is always maintained at 1.1–1.4. These results indicate that the restoration of sp^2 carbon in the CNFs/$[RGO]_n$ paper, which will favor electron transport. The characteristic Raman peak of cellulose is located at 1095 cm^{-1} (Bulota, Tanpichai, Hughes, & Eichhorn, 2012).

The surface contact angles of the CNFs, CNFs/$[Cu^{2+}/GO]_{20}$, CNFs/$[RGO]_{20}$ paper to water have been measured at ambient temperature and shown in Fig. 6c–e. The contact angles increases significantly from about 47° (CNFs paper) to about 75° (CNFs/$[GO]_{20}$ paper), and further increase to about 90° (CNFs/$[RGO]_{20}$ paper) after chemical reduction. Generally, CNFs paper is liable to dimensional instability because it is highly hygroscopic. The RGO active layers in the CNFs paper surface would impart not only high photoelectric properties but also act as moisture barriers to the CNFs paper which can significantly improve dimensional stability of CNFs/$[RGO]_n$ paper.

The roughness and uniformity are important parameters for the transparent conductive films (Zhang et al., 2006). That is because those parameters seriously affect the performance and life of the transparent conductive films. Fig. 6a shows the AFM images of CNFs and CNFs/$[RGO]_{20}$ paper. The R_{rms} (surface root-mean-square roughness) value of CNFs paper is 3.5–4.2 nm, which is consistent with the cellulose nanofiber diameter. The possible reason is that CNFs paper is composed of a layered structure of aligned CNFs, which are nearly parallel to the film's surface. Furthermore, the CNFs can be uniformly random orientated on the surface of CNFs paper. Fig. 6b shows the AFM image of CNFs/$[RGO]_{20}$ paper. It is easily to find that the entire surface morphology of the CNFs/$[RGO]_{20}$ paper generates significant changes after RGO uniformly covered in the CNFs paper. However, The R_{rms} value of the CNFs/$[RGO]_{20}$ paper increase to 5.1–6.0 nm after chemical reduction. The R_{rms} values become higher than CNFs paper maybe because wrinkling at the edges of RGO nanosheets. However, the wrinkling at the edges of RGO nanosheets (black arrow) (SEM image of CNFs/$[RGO]_{20}$ paper, Fig. S8) has a smooth contour. This phenomenon may be explained by the RGO nanosheets "bridging" effect at the wrinkling between the RGO nanosheets. GO nanosheets (the same layer or adjacent layers) are uniformly random interlocked by crosslinking agent-Cu^{2+}. Therefore, the GO nanosheets at the same layer can be effectively linked to each other by GO nanosheets of the adjacent layers. In addition, the GO nanosheets mostly position themselves with a lamellar structure. This lamellar structure of GO nanosheets in the CNFs/$[Cu^{2+}/GO]_{20}$ paper is free affected by the geometry of the GO nanosheets. After in situ chemical reduction, the lamellar structure can be maintained by van der waals or restoration π–π stacking between adjacent RGO layers. Such the RGO nanosheets lamellar structure can effectively provide the conductive channels. Thanks to the RGO nanosheets lamellar structure; the surface contact resistance of CNFs/$[RGO]_{20}$ paper can be significantly reduced.

Optoelectronic and mechanical properties are the most important properties for flexible transparent conductive films. Transmittance of the CNFs/$[RGO]_n$ paper at 550 nm is a function of the number of cycles (Fig. 7a), which decreases from 89.2% for pure CNFs paper to 76% for the CNFs/$[RGO]_{20}$ paper (inset of Fig. 7a).

Four-probe technique is used to measure the sheet resistance of CNFs/$[RGO]_n$ paper, and the results are shown in Fig. 7b.

The conductive channels have been formed in the CNFs/$[RGO]_0$ paper, which has a sheet resistance of ~1212.5 kΩ/□. The sheet resistance of the CNFs/$[RGO]_n$ paper rapidly decreases to ~2.5 kΩ/□ (n = 20) with the increase of the number of cycles, because the more conductive channels are formed. The bending stability is an important performance parameter of the flexible transparent conductive paper. Fig. 7c shows the bending stability of the CNFs/$[RGO]_{20}$ paper. The sheet resistance of the CNFs/$[RGO]_{20}$ paper is hardly changed with the increase of the bending cycles because the high-quality interface between the CNFs and RGO. The mechanical property of CNFs/$[RGO]_{20}$ paper is shown in Fig. 7d. Ultimate strength of the CNFs/$[RGO]_{20}$ paper is up to about 136 MPa, which is slightly lower than the CNFs paper (about 153 MPa). This indicates that the CNFs/$[RGO]_{20}$ paper inherits the excellent mechanical properties of CNFs paper. Meanwhile, the transparent conductive CNFs/$[RGO]_{20}$ paper also has excellent flexibility. In summary, the sheet resistance of the CNFs/$[RGO]_n$ paper significantly decreases with the increase of the number of cycles. And the sheet resistance of CNFs/$[RGO]_{20}$ paper is about 2.45 kΩ/□ at 76% transmittance (at 550 nm). The flexible transparent conductive CNFs/$[RGO]_n$ paper also has inherited the mechanical properties as well as excellent flexibility of the CNFs paper.

4. Conclusions

In this article, flexible transparent CNFs paper is used as the substrate of the transparent conductive paper. GO nanosheets can be uniformly immobilized in the CNFs paper surface by LbL assembly employing divalent Cu^{2+} ions as crosslinking agent. The active GO layer of CNFs/$[Cu^{2+}/GO]_{20}$ paper can be effectively and completely reduced by HI acid at 80 °C within 10 s. The resulted CNFs/$[RGO]_n$ paper has inherited the excellent mechanical properties of CNFs paper. The transmittance and sheet surface resistance of the CNFs/$[RGO]_n$ paper can be easily controlled by the number of LbL assembly. When the number of LbL assembly is 20, the paper has the sheet resistances of ~2.5 kΩ/□ and the transmittance is about 76% (at 550 nm). After bending 200 times, the sheet resistance nearly remains unchanged. The above advantages of the CNFs/$[RGO]_n$ flexible transparent conductive paper makes us believe that the CNFs/$[RGO]_n$ flexible transparent conductive paper (as an extremely important material) will be widely used in the next-generation flexible electronic devices. They will play a more important role in the field of information-transfer than conventional paper.

Acknowledgements

This work was financially supported by the Natural Science Foundation of Beijing, and Science and Technology Key Project of Beijing Municipal Education Commission.

Appendix A. Supplementary data

Supplementary data associated with this article can be found, in the online version, at http://dx.doi.org/10.1016/j.carbpol.2013.03.067.

References

Bai, H., Li, C., Wang, X., & Shi, G. (2011). On the gelation of graphene oxide. *Journal of Physical Chemistry C*, *115*(13), 5545–5551.

Bulota, M., Tanpichai, S., Hughes, M., & Eichhorn, S. J. (2012). Micromechanics of TEMPO-oxidized fibrillated cellulose composites. *ACS Applied Materials and Interfaces*, *4*(1), 331–337.

Chang, H., Wang, G., Yang, A., Tao, X., Liu, X., Shen, Y., et al. (2010). A transparent, flexible, low-temperature, and solution-processible graphene composite electrode. *Advanced Functional Materials*, *20*, 2893–2902.

Chen, W., Yu, H., Li, Q., Liu, Y., & Li, J. (2011). Ultralight and highly flexible aerogels with long cellulose I nanofibers. *Soft Matter*, *7*(21), 10360–10368.

Cote, L. J., Kim, F., & Huang, J. (2009). Langmuir–Blodgett assembly of graphite oxide single layers. *Journal of the American Chemical Society*, *131*(3), 1043–1049.

Creager, S. E., & Steiger, C. M. (1995). Conformational rigidity in a self-assembled monolayer of 4-mercaptobenzoic acid on gold. *Langmuir*, *11*(6), 1852–1854.

Dong, X. M., Revol, J. F., & Gray, D. G. (1998). Effect of microcrystallite preparation conditions on the formation of colloid crystals of cellulose. *Cellulose*, *5*(1), 19–32.

Eichhorn, S. J. (2011). Cellulose nanowhiskers: Promising materials for advanced applications. *Soft Matter*, *7*, 303–315.

Fukuzumi, H., Saito, T., Wata, T., Kumamoto, Y., & Isogai, A. (2009). CNFs transparent and high gas barrier films of cellulose nanofibers prepared by TEMPO-mediated oxidation. *Biomacromolecules*, *10*(1), 162–165.

Graf, D., Molitor, F., Ensslin, K., Stampfer, C., Jungen, A., Hierold, C., et al. (2007). Spatially resolved Raman spectroscopy of single- and few-layer graphene. *Nano Letters*, *7*(2), 238–242.

Holt, B. L., Stoyanov, S. D., Pelan, E., & Paunov, V. N. (2010). Novel anisotropic materials from functionalised colloidal cellulose and cellulose derivatives. *Journal of Materials Chemistry*, *20*, 10058–10070.

Hummers, W. S., & Offeman, R. E. (1958). Preparation of graphitic oxide. *Journal of the American Chemical Society*, *80*(6), 1339-1339

Isogai, A., Saito, T., & Fukuzumi, H. (2011). TEMPO-oxidized cellulose nanofibers. *Nanoscale*, *3*(1), 71–85.

Iwamoto, S., Kai, W., Isogai, A., & Iwata, T. (2009). Elastic modulus of single cellulose microfibrils from tunicate measured by atomic force microscopy. *Biomacromolecules*, *10*(9), 2571–2576.

Kaempgen, M., Duesberg, G. S., & Roth, S. (2005). Transparent carbon nanotube coatings. *Applied Surface Science*, *252*, 425–429.

Kao, C. Y., Lee, B., Wielunski, L. S., Heeney, M., McCulloch, I., Garfunkel, E., et al. (2009). Doping of conjugated polythiophenes with alky silanes. *Advanced Functional Materials*, *19*, 1906–1911.

Kumar, A., & Zhou, C. (2010). The race to replace tin-doped indium oxide: Which material will win? *ACS Nano*, *4*, 11–14.

Liu, Y.-T., Feng, Q.-P., Xie, X.-M., & Ye, X.-Y. (2011). The production of flexible and transparent conductive films of carbon nanotube/graphene networks coordinated by divalent metal (Cu, Ca or Mg) ions. *Carbon*, *49*(10), 3371–3375.

MacDonald, W. A. (2004). Engineered films for display technologies. *Journal of Materials Chemistry*, *14*(1), 4–10.

Marcano, D. C., Kosynkin, D. V., Berlin, J. M., Sinitskii, A., Sun, Z., Slesarev, A., et al. (2010). Improved synthesis of graphene oxide. *ACS Nano*, *4*(8), 4806–4814.

Nishino, T., Matsuda, I., & Hirao, K. (2004). All-cellulose composite. *Macromolecules*, *37*(20), 7683–7687.

Nogi, M., Iwamoto, S., Nakagaito, A. N., & Yano, H. (2009). Optically transparent nanofiber paper. *Advanced Materials*, *21*, 1595–1598.

Nomura, K., Ohta, H., Takagi, A., Kamiya, T., Hirano, M., & Hosono, H. (2004). Room-temperature fabrication of transparent flexible thin-film transistors using amorphous oxide semiconductors. *Nature*, *432*, 488–492.

Okita, Y., Saito, T., & Isogai, A. (2010). Entire surface oxidation of various cellulose microfibrils by TEMPO-mediated oxidation. *Biomacromolecules*, *11*(6), 1696–1700.

Paakko, M., Vapaavuori, J., Silvennoinen, R., Kosonen, H., Ankerfors, M., Lindstrom, T., et al. (2008). Long and entangled native cellulose I nanofibers allow flexible aerogels and hierarchically porous templates for functionalities. *Soft Matter*, *4*(12), 2492–2499.

Park, S., Lee, K.-S., Bozoklu, G., Cai, W., Nguyen, S. T., & Ruoff, R. S. (2008). Graphene oxide papers modified by divalent ions – Enhancing mechanical properties via chemical cross-linking. *ACS Nano*, *2*(3), 572–578.

Pei, S., Zhao, J., Du, J., Ren, W., & Cheng, H.-M. (2010). Direct reduction of graphene oxide films into highly conductive and flexible graphene films by hydrohalic acids. *Carbon*, *48*(15), 4466–4474.

Rathmell, A. R., & Wiley, B. J. (2011). The synthesis and coating of long, thin copper nanowires to make flexible, transparent conducting films on plastic substrates. *Advanced Materials*, *23*, 4798–4803.

Saito, T., Hirota, M., Tamura, N., Kimura, S., Fukuzumi, H., Heux, L., et al. (2009). Individualization of nano-sized plant cellulose fibrils by direct surface carboxylation using TEMPO catalyst under neutral conditions. *Biomacromolecules*, *10*(7), 1992–1996.

Saito, T., & Isogai, A. (2004). TEMPO-mediated oxidation of native cellulose. The effect of oxidation conditions on chemical and crystal structures of the water-insoluble fractions. *Biomacromolecules*, *5*(5), 1983–1989.

Saito, T., Kimura, S., Nishiyama, Y., & Isogai, A. (2007). Cellulose nanofibers prepared by TEMPO-mediated oxidation of native cellulose. *Biomacromolecules*, *8*, 2485–2491.

Saito, T., Nishiyama, Y., Putaux, J.-L., Vignon, M., & Isogai, A. (2006). Homogeneous suspensions of individualized microfibrils from TEMPO-catalyzed oxidation of native cellulose. *Biomacromolecules*, *7*(6), 1687–1691.

Saito, T., Uematsu, T., Kimura, S., Enomae, T., & Isogai, A. (2011). Self-aligned integration of native cellulose nanofibrils towards producing diverse bulk materials. *Soft Matter*, *7*(19), 8804–8809.

Shim, B. S., Zhu, J., Jan, E., Critchley, K., Ho, S., Podsiadlo, P., et al. (2009). Multiparameter structural optimization of single-walled carbon nanotube composites: Toward record strength, stiffness, and toughness. *ACS Nano*, *3*(7), 1711–1722.

Tung, V. C., Allen, M. J., Yang, Y., & Kaner, R. B. (2009). High-throughput solution processing of large-scale graphene. *Nature Nanotechnology*, *4*(1), 25–29.

Yu, Z., Zhang, Q., Li, L., Chen, Q., Niu, X., Liu, J., et al. (2011). Highly flexible silver nanowire electrodes for shape-memory polymer light-emitting diodes. *Advanced Materials*, *23*, 664–668.

Zhang, D., Ryu, K., Liu, X., Polikarpov, E., Ly, J., Tompson, M. E., et al. (2006). Transparent, conductive, and flexible carbon nanotube films and their application in organic light-emitting diodes. *Nano Letters*, *6*(9), 1880–1886.

Zhao, J., Pei, S., Ren, W., Gao, L., & Cheng, H.-M. (2010). Efficient preparation of large-area graphene oxide sheets for transparent conductive films. *ACS Nano*, *4*(9), 5245–5252.

Zhu, J., Shim, B. S., Di Prima, M., & Kotov, N. A. (2011). Transparent conductors from carbon nanotubes LBL-assembled with polymer dopant with pi–pi electron transfer. *Journal of the American Chemical Society*, *133*(19), 7450–7460.